

Structural transformation and ferroelectromagnetic behavior in single-phase $\text{Bi}_{1-x}\text{Nd}_x\text{FeO}_3$ multiferroic ceramics

G. L. Yuan and Siu Wing Or^{a)}

Department of Applied Physics, The Hong Kong Polytechnic University, Hung Hom, Kowloon, Hong Kong

J. M. Liu

Department of Applied Physics, The Hong Kong Polytechnic University, Hung Hom, Kowloon, Hong Kong and Laboratory of Solid State Microstructures, Nanjing University, Nanjing 210093, China

Z. G. Liu

Laboratory of Solid State Microstructures, Nanjing University, Nanjing 210093, China

(Received 18 April 2006; accepted 16 June 2006; published online 4 August 2006)

Single-phase $\text{Bi}_{1-x}\text{Nd}_x\text{FeO}_3$ (BNFO_x) ($x=0-0.2$) multiferroic ceramics were prepared to study the effects of Nd substitution on their crystal structure and ferroelectromagnetic behavior. Rietveld refinement of x-ray diffraction data showed a continual transformation of crystal structure from the rhombohedral structure of $\text{BNFO}_{x=0}$ (BiFeO_3) to a triclinic structure in $\text{BNFO}_{x=0.05-0.15}$ and a pseudotetragonal structure in $\text{BNFO}_{x=0.175-0.2}$. Ferroelectromagnetic measurements revealed the existence of ferroelectricity with remnant polarization of $\sim 9 \mu\text{C}/\text{cm}^2$ in $\text{BNFO}_{x=0-0.175}$, paraelectricity in $\text{BNFO}_{x=0.2}$, and weak ferromagnetism with remnant magnetizations of $0.07-0.227 \text{ emu/g}$ in $\text{BNFO}_{x=0.15-0.2}$. Magnetoelectric coupling was obvious in $\text{BNFO}_{x=0.15-0.175}$ near the Néel temperature of $\sim 380^\circ\text{C}$. © 2006 American Institute of Physics.

[DOI: 10.1063/1.2266992]

Single-phase BiFeO_3 is one of very important multiferroic materials characterized by the high Curie ($T_C \sim 830^\circ\text{C}$) and Néel ($T_N \sim 370^\circ\text{C}$) temperatures.¹⁻³ Extensive studies have been put on this bulk ceramic in recent years, yet three crucial problems have limited the release and measurements of simultaneous effects of ferroelectricity, piezoelectricity, and weak ferromagnetism. These problems include (1) difficulties in synthesizing single-phase samples due to the metastable state of BiFeO_3 and volatilization of Bi_2O_3 , (2) difficulties in imparting strong ferroelectric behavior and piezoelectric properties because of the low electrical resistivity, and (3) difficulties in deriving weak ferromagnetism owing to the cancellation of the possible nonzero remnant magnetization (M_r) permitted by the canted G -type antiferromagnetic order by the space-modulated spin structure.⁴⁻⁶

Recently, we have shown that problems 1 and 2 can be solved using a specific synthesis technique.^{7,8} To practically realize weak ferromagnetism (problem 3), Mathe *et al.* proposed to suppress the space-modulated spin structure of BiFeO_3 by A -site substitution of a smaller Nd^{3+} ion for Bi^{3+} ion.⁹ While structural, dielectric, and electrical properties of $\text{Bi}_{1-x}\text{Nd}_x\text{FeO}_3$ (BNFO_x) were obtained for various Nd concentration x of $0.2-1$, the effects of ferroelectricity and weak ferromagnetism were not addressed at all due to the extremely low resistivity and paraelectric nature of their samples.⁹ In this letter, we prepared single-phase BNFO_x bulk samples with x slightly varying in the ferroelectric-paraelectric transition region of $0-0.2$ (where $\text{BNFO}_{x=0}$ is BiFeO_3) and reported their crystal structure parameter changes, ferroelectricity-paraelectricity transition, weak ferromagnetism-antiferromagnetism interaction, and magnetoelectric coupling.

The specific synthesis technique that was adopted to prepare single-phase $\text{BNFO}_{x=0-0.15}$ samples was used to prepare $\text{BNFO}_{x=0-0.2}$ disk samples with diameter of 5 mm and thickness of 1 mm. This technique involved the use of high-purity ($>99\%$) Bi_2O_3 , Fe_2O_3 , and Nd_2O_3 powders of $<1 \mu\text{m}$ size and a rapid liquid-phase sintering process of 855°C for 20 min at high heating and cooling rate of 100 and 10°C/s , respectively.^{7,8,10}

The crystal structure of the sintered samples was examined by an x-ray diffractometer (Bruker D8) with a 2θ step size of 0.02° and at a scan rate of 1 step per 4 s. Simulation of crystal structure based on the measured x-ray diffraction (XRD) data was performed using a Rietveld crystal structure refinement software (FULLPROF 2000). The polarization hysteresis (P - E) loop was measured with a standard Sawyer-Tower circuit at 100 Hz. The magnetization hysteresis (M - H) loop was evaluated using a superconducting quantum interference device (Quantum Design XL7d). The temperature dependence of the relative dielectric constant (ϵ) and loss tangent ($\tan \delta$) was determined at 10 kHz using an impedance analyzer (Agilent 4294A).

Figure 1 shows the comparison between the measured and simulated XRD patterns of $\text{BNFO}_{x=0-0.2}$ samples. From the measured XRD patterns, all samples have a single-phase perovskite structure with no trace of other impurity phases (e.g., Fe_2O_3 , Bi_2O_3 , $\text{Bi}_2\text{Fe}_4\text{O}_9$, etc.) within the uncertainty of XRD.¹¹ From the two insets of Fig. 1, the sharp single peak of $\text{BNFO}_{x=0}$ undergoes a shift in 2θ and a split into two smaller peaks in $\text{BNFO}_{x=0.15-0.2}$ in the 2θ range of $21.5^\circ-23^\circ$, whereas the doubly split peaks of $\text{BNFO}_{x=0}$ overlap partially to form a broadened peak in $\text{BNFO}_{x=0.15-0.2}$ in the higher 2θ range of $31^\circ-33^\circ$. The observations suggest the existence of structural transformation with a continual change of crystal structure parameters in the samples.

^{a)}Electronic mail: apswor@polyu.edu.hk

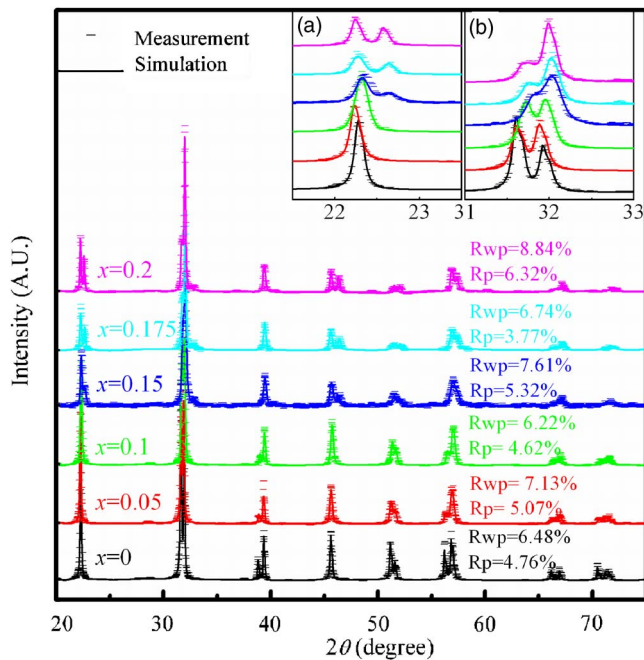


FIG. 1. (Color online) Comparison between the measured and simulated XRD patterns of $\text{BNFO}_{x=0-0.2}$ samples.

In order to further analyze such transformation, the measured XRD patterns of the samples were used in Rietveld refinement of crystal structures based on a triclinic structure, $P1$ space group, and a single cell with A -site Bi/Nd mixed atoms rather than a supercell. In more detail, since single-phase BiFeO_3 has a rhombohedral structure with $R3c$ space group at room temperature^{7,8,10} this highly symmetric structure can be treated as a special triclinic structure with comparatively lower symmetry. As a result, all the $\text{BNFO}_{x=0-0.2}$ samples were considered to have a triclinic structure in the refinement for ease of comparison of the refinement results. As shown in Fig. 1, the simulated XRD patterns coincide well with the measured XRD patterns with generally small R values (i.e., $\leq 8.84\%$ for R_{wp} and $\leq 6.32\%$ for R_p). Thus, our $\text{BNFO}_{x=0-0.2}$ samples should have a single-phase triclinic structure with $P1$ space group by nature, and $\text{BNFO}_{x=0}$ that possess a single-phase rhombohedral structure with $R3c$ space group in specific can be regarded as a special triclinic structure with $P1$ space group.

Figure 2 illustrates the refined crystal structure parameters as a function of x . The rhombohedral structure of $\text{BNFO}_{x=0}$ with crystal axes $a=b=c=3.942 \text{ \AA}$ and crystal axial angles $\alpha=\beta=\gamma=89.43^\circ$ is confirmed again in this study.^{7,10,11} A distortion of crystal structure from the rhombohedral structure of $\text{BNFO}_{x=0}$ to a triclinic structure (i.e., $a \neq b \neq c$; $\alpha \approx \beta > \gamma$) with larger crystal structure parameters occurs in $\text{BNFO}_{x=0.05}$. $\text{BNFO}_{x=0.1}$ also shows a triclinic structure even though its crystal structure parameters are subtle different from those of $\text{BNFO}_{x=0.05}$. $\text{BNFO}_{x=0.15}$ displays comparatively larger a , b , α , β , and γ values, besides a relatively smaller c value, than the rhombohedral structure of $\text{BNFO}_{x=0}$. This indicates that while $\text{BNFO}_{x=0.15}$ can be described by a triclinic structure, there is a tendency for it to transform to a pseudotetragonal structure with $a=b > c$ and $\alpha=\beta=\gamma=90^\circ$. Both $\text{BNFO}_{x=0.175}$ and $\text{BNFO}_{x=0.2}$ demonstrate a pseudotetragonallike structure with $a \approx b > c$ and $\alpha \approx \beta \approx \gamma \approx 90^\circ$ as a result of a primary tetragonal distortion plus a possible small triclinic distortion.⁹ Consequently,

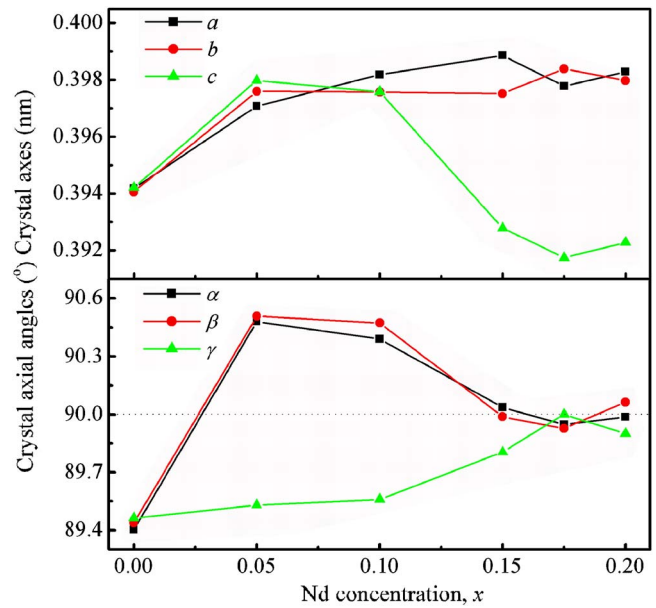


FIG. 2. (Color online) Refined crystal structure parameters of $\text{BNFO}_{x=0-0.2}$ samples as a function of Nd concentration x .

$\text{BNFO}_{x=0-0.2}$ transforms from rhombohedral structure at $x=0$ to triclinic structure at $x=0.05-0.15$ and finally to pseudotetragonal structure at $x=0.175-0.2$.

Figure 3 plots the polarization hysteresis (P - E) loops of $\text{BNFO}_{x=0}$, $\text{BNFO}_{x=0.1}$, $\text{BNFO}_{x=0.175}$, and $\text{BNFO}_{x=0.2}$ samples measured at 100 Hz. Obvious ferroelectric behavior with a large remnant polarization (P_r) of $\sim 9 \mu\text{C}/\text{cm}^2$ is observed in $\text{BNFO}_{x=0}$, $\text{BNFO}_{x=0.1}$, and $\text{BNFO}_{x=0.175}$, while paraelectric behavior is seen in $\text{BNFO}_{x=0.2}$. For the ferroelectric $\text{BNFO}_{x=0}$, $\text{BNFO}_{x=0.1}$, and $\text{BNFO}_{x=0.175}$, the maximum polarization (P_m) and electric field (E_m) are $19.7 \mu\text{C}/\text{cm}^2$ at $137 \text{ kV}/\text{cm}$, $18.1 \mu\text{C}/\text{cm}^2$ at $139 \text{ kV}/\text{cm}$, and $19.1 \mu\text{C}/\text{cm}^2$ at $143 \text{ kV}/\text{cm}$, respectively. These ferroelectric P_m values are significantly larger than the paraelectric P_m of $1.9 \mu\text{C}/\text{cm}^2$ even at a higher E_m of $145 \text{ kV}/\text{cm}$ in $\text{BNFO}_{x=0.2}$. The results suggest that the stereochemical activ-

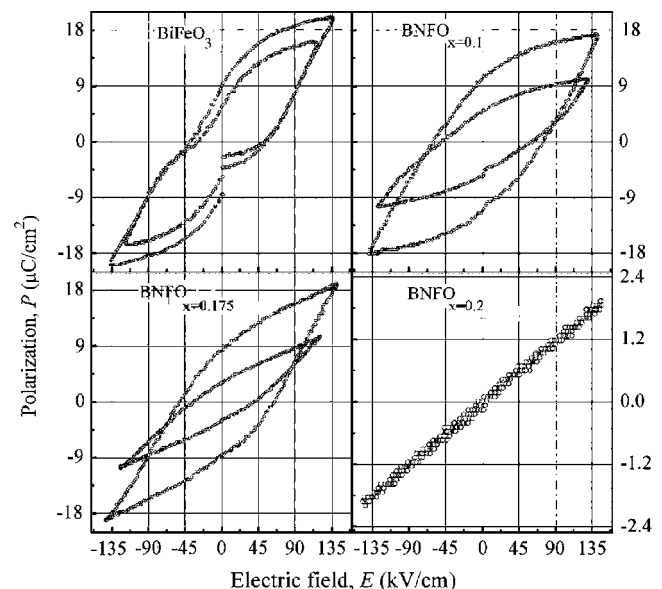


FIG. 3. Polarization hysteresis (P - E) loops of (a) $\text{BNFO}_{x=0}$ (BiFeO_3), (b) $\text{BNFO}_{x=0.1}$, (c) $\text{BNFO}_{x=0.175}$, and (d) $\text{BNFO}_{x=0.2}$ samples.

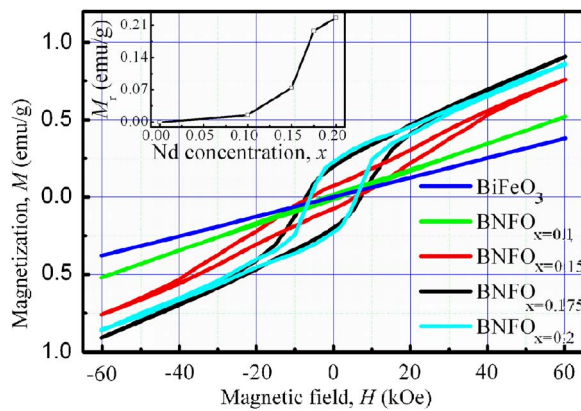


FIG. 4. (Color online) Magnetization hysteresis (M - H) loops of $\text{BNFO}_{x=0-0.2}$ samples.

ity of the Bi lone electron pair plays an important role in the transition from ferroelectricity to paraelectricity at $0.175 < x < 0.2$.^{1,3} In conventional ferroelectric perovskites, the ferroelectric distortion is stabilized by charge transfer from the oxygen to the unoccupied transition metal d orbitals. Although Bi^{3+} ion has been partially substituted by Nd^{3+} ion in our $\text{BNFO}_{x=0-0.175}$ samples, a lone s^2 pair of electrons of a Bi^{3+} ion may hybridize with an empty p orbital of Bi^{3+} or an O^{2-} ion to form a localized lobe, resulting in the non-centrosymmetric distortion and hence ferroelectricity.^{1,3} Further increase in x towards 0.175 tends to weaken the stereochemical activity of the Bi lone electron pair, leading to a ferroelectric-paraelectric transition at $0.175 < x < 0.2$. As the crystal structure parameters only change slowly in the x range of 0.175–0.2, the stereochemical activity should have the predominant effect on the observed ferroelectric-paraelectric transition.

Figure 4 shows the magnetization hysteresis (M - H) loops of $\text{BNFO}_{x=0-0.2}$ samples for the maximum magnetic field (H_m) of 60 kOe. It is evident that the antiferromagnetism intrinsic in $\text{BNFO}_{x=0}$ becomes weak ferromagnetism with a small but nonzero M_r of ≤ 0.227 emu/g in $\text{BNFO}_{x=0.1-0.2}$. From the inset of Fig. 4, M_r essentially vanishes in $\text{BNFO}_{x=0}$; it exhibits a slow increasing trend from zero for $x \leq 0.1$ before displaying a relatively rapid rise from 0.015 to 0.227 emu/g when x is increased from 0.1 to 0.2. In fact, the crystal structure parameters change dramatically in the x range of 0.1–0.175, as evidenced in Fig. 2. The continuing increase in M_r in our samples is likely due to the continuing collapse of the space-modulated spin structure of $\text{BNFO}_{x=0}$.¹² Indeed, the transformation from the rhombohedral structure in $\text{BNFO}_{x=0}$ to triclinic structure in $\text{BNFO}_{x=0.05-0.15}$ and then to pseudotetragonal structure in $\text{BNFO}_{x=0.175-0.2}$ gives rise to the continuing collapse of the space-modulated spin structure.^{4-6,12}

Figure 5 shows the temperature dependence of relative dielectric constant (ϵ) and loss tangent ($\tan \delta$) at 10 kHz for $\text{BNFO}_{x=0.175}$ and $\text{BNFO}_{x=0.2}$ samples. It is found that $\text{BNFO}_{x=0.175}$ has dielectric anomalies at T_N of ~ 380 °C, which is similar to those of $\text{BNFO}_{x=0}$ at T_N of ~ 370 °C and suggests the presence of magnetoelectric coupling in $\text{BNFO}_{x=0.175}$ for temperatures below ~ 380 °C.^{1,13-15} However, dielectric anomalies are not detected in $\text{BNFO}_{x=0.2}$ in the whole temperature range of

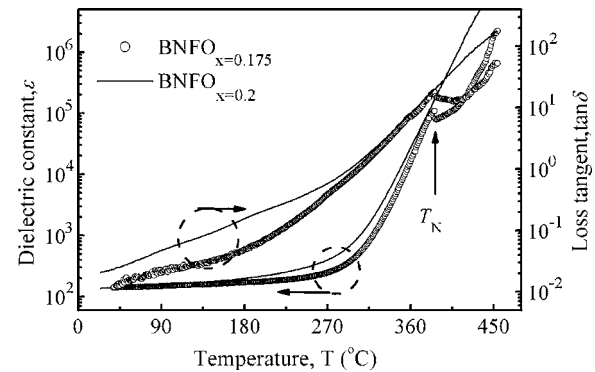


FIG. 5. Dependence of relative dielectric constant (ϵ) and loss tangent ($\tan \delta$) for $\text{BNFO}_{x=0.175}$ and $\text{BNFO}_{x=0.2}$ samples.

40–450 °C.⁹ As found in Fig. 3, $\text{BNFO}_{x=0.2}$ is paraelectric rather than ferroelectric; it should not display any magneto-electric coupling, i.e., the origin of dielectric anomalies near T_N .

In conclusion, we have found that single-phase BNFO_x multiferroic ceramics have a rhombohedral structure at $x=0$, a triclinic structure at $x=0.05-0.15$, and a pseudotetragonal structure at $x=0.175-0.2$. The ferroelectric-paraelectric transition occurred at $0.175 < x < 0.2$ mainly results from the weakening of the stereochemical activity of the Bi lone electron pair. Due to the transformation of crystal structure, the space-modulated spin structure in $\text{BNFO}_{x=0}$ collapses continuously with increasing x and eventually releases weak ferromagnetism at $x=0.15-0.2$. The coexistence of ferroelectricity and weak ferromagnetism in $\text{BNFO}_{x=0.15-0.175}$ allows significant magnetoelectric coupling near the Néel temperature of ~ 380 °C.

This work was supported by the Hong Kong Research Grants Council (PolyU 5255/03E) and the National Natural Science Foundation of China (10374048 and 50502018).

¹M. Fiebig, J. Phys. D **38**, R123 (2005).

²J. Wang, J. B. Neaton, H. Zheng, V. Nagarajan, S. B. Ogale, B. Liu, D. Viehland, V. Vaithyanathan, D. G. Schlom, U. V. Waghmare, N. A. Spaldin, K. M. Rabe, M. Wuttig, and R. Ramesh, Science **299**, 1719 (2003).

³R. Seshadri and A. Nicola, Chem. Mater. **13**, 2892 (2001).

⁴A. V. Zaleskiĭ, A. A. Frolov, T. A. Khimich, and A. A. Bush, Phys. Solid State **45**, 141 (2003).

⁵B. Ruetter, S. Zvyagin, A. P. Pyatakov, A. Bush, J. F. Li, V. I. Belotelov, A. K. Zvezdin, and D. Viehland, Phys. Rev. B **69**, 064114 (2004).

⁶F. Bai, J. Wang, M. Wuttig, J. Li, N. Wang, A. P. Pyatakov, A. K. Zvezdin, L. E. Cross, and D. Viehland, Appl. Phys. Lett. **86**, 032511 (2005).

⁷G. L. Yuan, S. W. Or, Y. P. Wang, Z. G. Liu, and J. M. Liu, Solid State Commun. **138**, 76 (2006).

⁸G. L. Yuan and S. W. Or, Appl. Phys. Lett. **88**, 062905 (2006).

⁹V. L. Mathe, K. K. Patankar, R. N. Patil, and C. D. Lokhande, J. Magn. Magn. Mater. **270**, 380 (2004).

¹⁰Y. P. Wang, L. Zhou, M. F. Zhang, X. Y. Chen, J.-M. Liu, and Z. G. Liu, Appl. Phys. Lett. **84**, 1731 (2004).

¹¹H. Béa, M. Bibes, A. Barthélémy, K. Bouzouane, E. Jacquet, A. Khodan, J.-P. Contour, S. Fusil, F. Wyczisk, A. Forget, D. Lebeugle, D. Colson, and M. Viret, Appl. Phys. Lett. **87**, 072508 (2005).

¹²D. Lee, M. G. Kim, S. Ryu, H. M. Jang, and S. G. Lee, Appl. Phys. Lett. **86**, 222903 (2005).

¹³V. R. Palkar, K. G. Kumara, and S. K. Malik, Appl. Phys. Lett. **84**, 2856 (2004).

¹⁴V. R. Palkar, D. C. Kundaliy, S. K. Malik, and S. Bhattachary, Phys. Rev. B **69**, 212102 (2004).

¹⁵L. Benguigui, Solid State Commun. **11**, 825 (1972).